MJFAS MALAYSIAN JOURNAL OF FUNDAMENTAL AND APPLIED SCIENCES
PRINT ISSN: 2289-5981 | ONLINE ISSN: 2289-599X

RESEARCH ARTICLE

Mixed convection boundary layer flow on a horizontal circular cylinder in a nanofluid with viscous dissipation effect

Muhammad Khairul Anuar Mohamed [a, b, *], Norhafizah Md Sarif [b], Nor Aida Zuraimi Md Noar [b], Mohd Zuki Salleh [b], Anuar Mohd Ishak [c]

[a] *Centre of Inter Disciplinary Studies, DRB-HICOM University of Automotive Malaysia, Peramu Jaya Industrial Area, 26607 Pekan, Pahang, Malaysia*
[b] *Applied & Industrial Mathematics Research Group, Faculty of Industrial Science and Technology, Universiti Malaysia Pahang, 26300 UMP Kuantan, Pahang, Malaysia*
[c] *School of Mathematical Sciences, Faculty of Science & Technology, Universiti Kebangsaan Malaysia, 43600 UKM Bangi, Selangor, Malaysia*

* *Corresponding author: khairul.anuar@dhu.edu.my*

Article history
Submitted 13 October 2017
Revised 2 January 2018
Accepted 17 January 2018
Published Online 8 March 2018

Abstract

In this study, the mathematical modeling for the mixed convection boundary layer flow past a horizontal circular cylinder in a nanofluid with the presence of viscous dissipation effect is considered. The system of governing non-linear partial differential equations are first transformed to a more convenient form before being solved numerically using the Keller-box method. Numerical solutions are obtained for the reduced Nusselt number, Sherwood number and skin friction coefficient as well as the concentration, the temperature and the velocity profiles. The features of the flow and heat transfer characteristics for various values of the Eckert number, Lewis number, Brownian motion parameter, thermophoresis parameter, mixed convection parameter, concentration mixed convection parameter and Prandtl number are analyzed and discussed. It is suggested that the presence of buoyancy forces in mixed convection delayed the separation in assisting flow. Further, the Nusselt number decreases while Sherwood number increases with the increase of Brownian parameter, thermophoresis parameter and the Lewis number. It is worth mentioning that the results in this paper is important especially in understanding the nanofluid parameters behaviour as cooling medium in such applications like transformer liquid submersion system, power supply unit in supercomputer and liquid cooling for electronic components like capacitor and transistor.

***Keywords*:** Mixed convection, circular cylinder, nanofluid, viscous dissipation

INTRODUCTION

The convective flow and heat transfer of a nanofluid have become a common topic discussed nowadays. Nanofluid is experimental proven enhanced the thermal conductivity, viscosity, thermal diffusivity and convective heat transfer compared to those base fluids like water and oil. It is applied widely in many applications for example as coolant medium in tire production and nuclear reactor, act as a smart fluid in battery devices, as a coolant in a car radiator, brake fluid, fuel catalyst to improve engine combustion and also act to cooling a microchip in electronic devices (Wong and De Leon, 2010). Many researchers have considered nanofluid as a medium of convective boundary layer flow in their studies such as Tham and Nazar (2012), Anwar *et al.* (2013), Roşca and Pop (2014), Mohamed *et al.* (2015), Hussanan *et al.* (2016) who investigated the steady and unsteady flow on stagnation point flow, stretching sheet, vertical surface, moving surface and solid sphere all filled with nanofluid, respectively. Recently, Jan *et al.* (2017), Khan (2017) and Kho *et al.* (2017) studied the thermal radiation and slip effect on MHD flow over a stretching surface and spherical shape which immersed in Williamson and engine oil nano liquid with molybdenum disulphide nanoparticles.

The governing equations for the model of mixed convection on horizontal circular cylinder was solved numerically by Merkin (1977). The solution was obtained for $\Pr = 1$ and it was found that there exists a separation where there is no solution or the laminar boundary layer equations are not valid after the separation point. Jain and Lohar (1979) considered the unsteady case for this topic. The variations of mean Nusselt number with time were shown and discussed. The unsteady case with the introduction of double diffusion within a porous medium was then studied by Kumari and Nath (1989) while Aldoss *et al.* (1996) considered the magnetohydrodynamic (MHD) effects. Next, Nazar *et al.* (2003) extended the work by Merkin (1977) to a micropolar fluid while Anwar *et al.* (2008) considered the similar problem for a viscoelastic fluid. The point of separation for the boundary layer, effects of Prandtl number and mixed convection parameter were discussed. Both problems were solved by using the Keller-box method. Further, Salleh *et al.* (2010) investigated the mixed convection boundary layer flow past a horizontal circular cylinder with Newtonian heating boundary condition. Other researchers who considered this topic including Ahmad *et al.* (2009), Nazar *et al.* (2011), Rashad *et al.* (2013) and Roşca *et al.* (2014) who studied the effect of temperature dependent viscosity on the mixed convection flows past a horizontal

circular cylinder embedded in a porous medium filled by a nanofluid with convective boundary condition and dual solutions for the mixed convection boundary layer flow close to the lower stagnation point of a horizontal circular cylinder, respectively. Recently, Udhayakumar *et al.* (2016) and Mohamed *et al.* (2016) solved the effects of viscous dissipation and magnetohydrodynamic on the mixed convection over an isothermal circular cylinder in viscous and nanofluid, respectively.

In many investigations above, the viscous dissipations is neglected. According to Gebhart (1962), the viscous dissipation or internal friction is the rate of the work done againts viscous forces is irreversibly converted into internal energy. It is known that the effect of viscous dissipation is significant especially for high velocity flow. The characteristics of the viscous dissipation are commonly represented by Eckert number which usually denoted as Ec.

Therefore, based on the above-mentioned studies, this paper investigates the effect of viscous dissipation on the mixed convection boundary layer flow past a horizontal circular cylinder in a nanofluid with constant wall temperature (CWT). To the best of our knowledge, this problem has never been considered before, so that the results reported here are new.

MATHEMATICAL FORMULATIONS

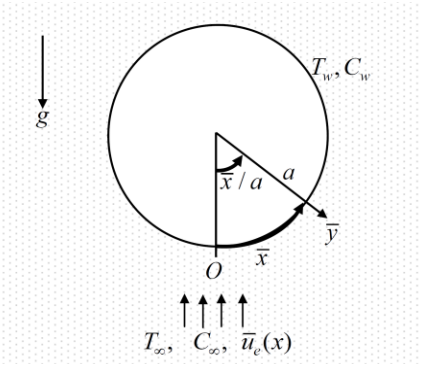

Fig. 1 Physical model of the coordinate system.

Consider a horizontal circular cylinder of radius a, which is heated to a constant temperature T_w and embedded in a nanofluid with ambient temperature T_∞ as shown in Fig. 1. The orthogonal coordinates of $\bar{x}$ and $\bar{y}$ are measured along the cylinder surface, starting with the lower stagnation point $\bar{x}=0$, and normal to it, respectively. Under the assumption that the boundary layer approximations is valid, the dimensional governing equations of mixed convection boundary layer flow are (Merkin, 1977; Nazar *et al.*, 2003; Salleh *et al.*, 2010):

$$\frac{\partial \bar{u}}{\partial \bar{x}}+\frac{\partial \bar{v}}{\partial \bar{y}}=0, \tag{1}$$

$$\bar{u}\frac{\partial \bar{u}}{\partial \bar{x}}+\bar{v}\frac{\partial \bar{u}}{\partial \bar{y}}=\bar{u}_e\frac{d\bar{u}_e}{d\bar{x}}+\nu\frac{\partial^2 \bar{u}}{\partial \bar{y}^2}+g\beta(T-T_\infty)\sin\frac{\bar{x}}{a}+g\beta_c\left(C-C_\infty\right)\sin\frac{\bar{x}}{a}, \tag{2}$$

$$\bar{u}\frac{\partial T}{\partial \bar{x}}+\bar{v}\frac{\partial T}{\partial \bar{y}}=\alpha\frac{\partial^2 T}{\partial \bar{y}^2}+\tau\left[D_B\frac{\partial C}{\partial \bar{y}}\frac{\partial T}{\partial \bar{y}}+\frac{D_T}{T_\infty}\left(\frac{\partial T}{\partial \bar{y}}\right)^2\right]+\frac{\mu}{\rho C_p}\left(\frac{\partial \bar{u}}{\partial \bar{y}}\right)^2, \tag{3}$$

$$\bar{u}\frac{\partial C}{\partial \bar{x}}+\bar{v}\frac{\partial C}{\partial \bar{y}}=D_B\frac{\partial^2 C}{\partial \bar{y}^2}+\frac{D_T}{T_\infty}\frac{\partial^2 T}{\partial \bar{y}^2}, \tag{4}$$

subject to the boundary conditions

$$\bar{u}(\bar{x},0)=\bar{v}(\bar{x},0)=0,\ T(\bar{x},0)=T_w,\ C(\bar{x},0)=C_w,$$
$$\bar{u}(\bar{x},\infty)\to\bar{u}_e,\ T(\bar{x},\infty)\to T_\infty,\ C(\bar{x},\infty)\to C_\infty \tag{5}$$

where $\bar{u}$ and $\bar{v}$ are the velocity components along the $\bar{x}$ and $\bar{y}$ axes, respectively. μ is the dynamic viscosity, ν is the kinematic viscosity, g is the gravity acceleration, β and β_c are the thermal and concentration expansion coefficient, T is the local temperature, ρ is the fluid density and C_p is the specific heat capacity at a constant pressure.

Furthermore, C_w is the nanoparticle volume fraction C at the surface, C_∞ is the ambient nanoparticle volume fraction, D_B is the Brownian diffusion coefficient, D_T is the thermophoresis diffusion coefficient, τ is the ratio of the effective heat capacity of the nanoparticle material and the heat capacity of the base fluid. The external flow $\bar{u}_e(x)$ is given by

$$\bar{u}_e(x)=U_\infty\sin\left(\frac{\bar{x}}{a}\right) \tag{6}$$

Next, the governing Eqs. (1) – (4) are first transformed to non-dimensional form, therefore the following non-dimensional variables are introduced:

$$x=\frac{\bar{x}}{a},\ y=\mathrm{Re}^{1/2}\frac{\bar{y}}{a},\ u=\frac{\bar{u}}{U_\infty},\ v=\mathrm{Re}^{1/2}\frac{\bar{v}}{U_\infty},$$
$$\theta(x,y)=\frac{T-T_\infty}{T_w-T_\infty},\ \phi(x,y)=\frac{C-C_\infty}{C_w-C_\infty},\ u_e(x)=\frac{\bar{u}_e(x)}{U_\infty}. \tag{7}$$

where θ and ϕ are the rescaled dimensionless temperature and nanoparticle volume fraction of the fluid and $\mathrm{Re}=\frac{U_\infty a}{\nu}$ is Reynolds number. Then Eqs. (1) – (4) becomes

$$\frac{\partial u}{\partial x}+\frac{\partial v}{\partial y}=0, \tag{8}$$

$$u\frac{\partial u}{\partial x}+v\frac{\partial u}{\partial y}=u_e\frac{du_e}{dx}+\frac{\partial^2 u}{\partial y^2}+\lambda\theta\sin x+\omega\phi\sin x, \tag{9}$$

$$u\frac{\partial \theta}{\partial x}+v\frac{\partial \theta}{\partial y}=\frac{1}{\mathrm{Pr}}\frac{\partial^2\theta}{\partial y^2}+N_b\frac{\partial\phi}{\partial y}\frac{\partial\theta}{\partial y}+N_t\left(\frac{\partial\theta}{\partial y}\right)^2+Ec\left(\frac{\partial u}{\partial y}\right)^2, \tag{10}$$

$$u\frac{\partial \phi}{\partial x}+v\frac{\partial \phi}{\partial y}=\frac{D_B}{\nu}\frac{\partial^2\phi}{\partial y^2}+\frac{D_T\left(T_w-T_\infty\right)}{T_\infty\nu\left(C_w-C_\infty\right)}\frac{\partial^2\theta}{\partial y^2} \tag{11}$$

where $\lambda=\frac{Gr}{\mathrm{Re}^2}$ is the mixed convection parameter, $\omega=\frac{Gr_c}{\mathrm{Re}^2}$ is the concentration mixed convection parameter, $Gr=\frac{g\beta(T_w-T_\infty)a^3}{\nu^2}$ is the Grashof number, $Gr_c=\frac{g\beta_c(C_w-C_\infty)a^3}{\nu^2}$ is the mass transfer Grashof number, $\mathrm{Pr}=\frac{\nu}{\alpha}$ is the Prandtl number, $N_b=\frac{\tau D_B(C_w-C_\infty)}{\nu}$ is the Brownian motion parameter, $N_t=\frac{\tau D_T(T_w-T_\infty)}{T_\infty\nu}$ is the thermophoresis parameter and $Ec=\frac{U_\infty{}^2}{C_p\left(T_w-T_\infty\right)}$ is the Eckert number. The Eq. (5) are transformed to

$$u(x,0)=0,\ v(x,0)=0,\ \theta(x,0)=1,\ \phi(x,0)=1,$$
$$u(x,\infty)\to u_e,\ \theta(x,\infty)\to 0,\ \phi(x,\infty)\to 0 \tag{12}$$

Eqs. (8)-(11) contain many dependent variables which make the set of equations difficult to solve. Hence, the following non-similarity functions are introduced:

$$\psi = xf(x,y),\ \ \phi = \phi(x,y),\ \ \theta = \theta(x,y), \tag{13}$$

where ψ is the stream function defined as $u = \frac{\partial \psi}{\partial y}$ and $v = -\frac{\partial \psi}{\partial x}$ which identically satisfies (8). By substituted Eq. (13) into Eqs. (8)-(11), the following partial differential equations are obtained:

$$\frac{\partial^3 f}{\partial y^3} + f\frac{\partial^2 f}{\partial y^2} - \left(\frac{\partial f}{\partial y}\right)^2 + \frac{\sin x}{x}\left(\lambda\theta + \omega\phi + \cos x\right) = x\left(\frac{\partial f}{\partial y}\frac{\partial^2 f}{\partial x \partial y} - \frac{\partial f}{\partial x}\frac{\partial^2 f}{\partial y^2}\right), \tag{14}$$

$$\frac{1}{\Pr}\frac{\partial^2 \theta}{\partial y^2} + f\frac{\partial \theta}{\partial y} + N_b\frac{\partial \phi}{\partial y}\frac{\partial \theta}{\partial y} + N_t\left(\frac{\partial \theta}{\partial y}\right)^2 = x\left(\frac{\partial f}{\partial y}\frac{\partial \theta}{\partial x} - \frac{\partial f}{\partial x}\frac{\partial \theta}{\partial y} - xEc\left(\frac{\partial^2 f}{\partial y^2}\right)^2\right). \tag{15}$$

$$\frac{\partial^2 \phi}{\partial y^2} + \frac{N_t}{N_b}\frac{\partial^2 \theta}{\partial y^2} + Lef\frac{\partial \phi}{\partial y} = xLe\left(\frac{\partial f}{\partial y}\frac{\partial \phi}{\partial x} - \frac{\partial f}{\partial x}\frac{\partial \phi}{\partial y}\right), \tag{16}$$

where $Le = \frac{\nu}{D_B}$ is the Lewis number. The boundary conditions (12) becomes

$$f(x,0) = \frac{\partial f}{\partial y}(x,0) = 0,\ \ \theta(x,0) = 1,\ \ \phi(x,0) = 1,$$
$$\frac{\partial f}{\partial y}(x,\infty) \to \frac{\sin x}{x},\ \ \theta(x,\infty) \to 0,\ \ \phi(x,\infty) \to 0 \tag{17}$$

The physical quantities of interest are the skin friction coefficient C_f, the local Nusselt number Nu_x and the local Sherwood number Sh_x which are given by

$$C_f = \frac{\tau_w}{\rho U_\infty^{\ 2}},\ \ Nu_x = \frac{aq_w}{k(T_w - T_\infty)},\ \ Sh_x = \frac{aj_w}{D_B(C_w - C_\infty)}. \tag{18}$$

The surface shear stress τ_w, the surface heat flux q_w and the surface mass flux j_w are given by

$$\tau_w = \mu\left(\frac{\partial \bar{u}}{\partial \bar{y}}\right)_{\bar{y}=0},\ \ q_w = -k\left(\frac{\partial T}{\partial \bar{y}}\right)_{\bar{y}=0},\ \ j_w = -D_B\left(\frac{\partial C}{\partial \bar{y}}\right)_{\bar{y}=0}, \tag{19}$$

with k being the thermal conductivity, respectively. Using Eqs. (7) and (13) give

$$C_f\,\mathrm{Re}_x^{1/2} = \left(x\frac{\partial^2 f}{\partial y^2}\right)_{\bar{y}=0},\ \ Nu_x\,\mathrm{Re}_x^{-1/2} = -\left(\frac{\partial \theta}{\partial y}\right)_{\bar{y}=0}$$
$$\text{and}\ \ Sh_x\,\mathrm{Re}_x^{-1/2} = -\left(\frac{\partial \phi}{\partial y}\right)_{\bar{y}=0}. \tag{20}$$

RESULTS AND DISCUSSION

The partial differential equations (14)-(16) subject to the boundary conditions (17) were solved numerically using the Keller-box method. Keller-box method is found to be powerful, efficient, easy to use and very suitable to solve the non-linear parabolic partial differential equation. Further, it can be modified to solve problem in any order. Seven parameters were considered, namely the Prandtl number Pr,the mixed convection parameter λ, the concentration mixed convection parameter ω, the Brownian motion parameter N_b, the thermophoresis parameter N_t, the Lewis number Le and the Eckert number Ec. The step size $\Delta y = 0.02$, $\Delta x = 0.005$ and the boundary layer thickness $y_\infty = 8$ and $x_\infty = \pi$ are used in obtaining the numerical results. Table 1 shows the comparison values of the reduced Nusselt number $Nu_x\,\mathrm{Re}_x^{-1/2}$ with previous results for various values of x. From Table 1, it is seen that the results are in a very good agreement therefore, it is concluded that Keller-box method works efficiently and provides accurate results for the present problem.

Tables 2 and 3 present the values of the reduced Nusselt number $Nu_x\,\mathrm{Re}_x^{-1/2}$ and the reduced Sherwood number $Sh_x\,\mathrm{Re}_x^{-1/2}$ with various values of x and λ. From both tables, it is found that the increase of x results in the decrease of $Nu_x\,\mathrm{Re}_x^{-1/2}$ and $Sh_x\,\mathrm{Re}_x^{-1/2}$. At a stagnation region $(x = 0)$, $Nu_x\,\mathrm{Re}_x^{-1/2}$ and $Sh_x\,\mathrm{Re}_x^{-1/2}$ achieve their maximum values. Physically, both quantities decrease which means the reduction in convective heat and mass transfer capabilities across the cylinder surface. As tables goes to the right, the value of $Nu_x\,\mathrm{Re}_x^{-1/2}$ and $Sh_x\,\mathrm{Re}_x^{-1/2}$ increase with λ. From the numerical results, as expected the opposing buoyancy flow shows a separation which contribute to turbulence flow. From the numerical calculations, it is found that the increase of λ delays the boundary layer separation (Merkin , 1977). Further, it is suggested that $\lambda \geq 1$ gives no separation to the boundary layer flow.

Table 1 Comparison values of $Nu_x\,\mathrm{Re}_x^{-1/2}$ with previous published results for various values of x and λ when $\Pr = 1,\ N_b = N_t = Le = \omega = Ec = 0$.

x/λ	-1.0			0			1.0		
	Nazar (2003)	Merkin (1977)	Present	Nazar (2003)	Merkin (1977)	Present	Nazar (2003)	Merkin (1977)	Present
0	0.5080	0.5067	0.5067	0.5710	0.5705	0.5705	0.6160	0.6156	0.6156
0.2	0.5022	0.5018	0.5015	0.5658	0.5658	0.5668	0.6125	0.6115	0.6125
0.4	0.4862	0.4865	0.4859	0.5560	0.5564	0.5562	0.6031	0.6028	0.6036
0.6	0.4584	0.4594	0.4585	0.5380	0.5391	0.5387	0.5880	0.5885	0.5890
0.8	0.4140	0.4160	0.4144	0.5130	0.5145	0.5139	0.5673	0.5686	0.5687
1.0	0.3259	0.3326	0.3281	0.4808	0.4826	0.4817	0.5414	0.5435	0.5432
1.2				0.4406	0.4426	0.4414	0.5105	0.5133	0.5126
1.4				0.3909	0.3928	0.3912	0.4750	0.4785	0.4774
1.6				0.3262	0.3280	0.3258	0.4354	0.4394	0.4381
1.8				0.2049	0.2114	0.2043	0.3924	0.3967	0.3951
2.0							0.3465	0.3509	0.3492
2.2							0.3002	0.3029	0.3013
2.4							0.2515	0.2540	0.2526
2.6							0.2040	0.2061	0.2051
2.8							0.1636	0.1634	0.1632
3.0							0.1397	0.1354	0.1364
π							0.1380	0.1306	0.1323

Table 2 Values of $Nu_x \operatorname{Re}_x^{-1/2}$ with various values of x and λ when $\Pr = 1,\ N_b = N_t = \omega = Ec = 0.1$ and $Le = 10$.

x/λ	-1.0	-0.5	0	0.5	1.0	2.0
0	0.4487	0.4806	0.5062	0.5278	0.5467	0.5789
0.2	0.4431	0.4755	0.5010	0.5224	0.5409	0.5721
0.4	0.4259	0.4610	0.4865	0.5072	0.5247	0.5531
0.6	0.4000	0.4379	0.4640	0.4838	0.4998	0.5240
0.8	0.3598	0.4074	0.4351	0.4544	0.4687	0.4878
1.0	0.2906	0.3695	0.4017	0.4213	0.4341	0.4478
1.2		0.3214	0.3647	0.3863	0.3984	0.4072
1.4		0.2452	0.3238	0.3508	0.3636	0.3688
1.6			0.2753	0.3148	0.3304	0.3341
1.8			0.2026	0.2772	0.2989	0.3040
2.0				0.2354	0.2685	0.2780
2.2				0.1831	0.2383	0.2555
2.4					0.2077	0.2353
2.6					0.1774	0.2163
2.8					0.1497	0.1978
3.0					0.1293	0.1784
π					0.1219	0.1628

Table 3 Values of $Sh_x \operatorname{Re}_x^{-1/2}$ with various values of x and λ when $\Pr = 1,\ N_b = N_t = \omega = Ec = 0.1$ and $Le = 10$.

x/λ	-1.0	-0.5	0	0.5	1.0	2.0
0	1.1085	1.2185	1.3043	1.3756	1.4370	1.5402
0.2	1.0959	1.2092	1.2969	1.3695	1.4321	1.5370
0.4	1.0551	1.1818	1.2752	1.3518	1.4173	1.5271
0.6	0.9891	1.1346	1.2383	1.3214	1.3920	1.5096
0.8	0.8770	1.0645	1.1845	1.2773	1.3549	1.4830
1.0	0.6627	0.9660	1.1120	1.2183	1.3049	1.4460
1.2		0.8257	1.0183	1.1434	1.2414	1.3974
1.4		0.5840	0.8994	1.0521	1.1684	1.3368
1.6			0.7448	0.9441	1.0742	1.2646
1.8			0.5060	0.8188	0.9729	1.1821
2.0				0.6736	0.8631	1.0917
2.2				0.4953	0.7481	0.9959
2.4					0.6323	0.8979
2.6					0.5218	0.7997
2.8					0.4256	0.7022
3.0					0.3570	0.6026
π					0.3317	0.5260

Table 4 Values of $Nu_x \operatorname{Re}_x^{-1/2}$ and $Sh_x \operatorname{Re}_x^{-1/2}$ for various values of x and ω when $\Pr = 1,\ \lambda = 1,\ N_b = N_t = Ec = 0.1$ and $Le = 10$.

x/ω	-1.0		-0.5		0	
	$Nu_x \operatorname{Re}_x^{-1/2}$	$Sh_x \operatorname{Re}_x^{-1/2}$	$Nu_x \operatorname{Re}_x^{-1/2}$	$Sh_x \operatorname{Re}_x^{-1/2}$	$Nu_x \operatorname{Re}_x^{-1/2}$	$Sh_x \operatorname{Re}_x^{-1/2}$
0	0.5298	1.3704	0.5378	1.4020	0.5452	1.4314
0.2	0.5244	1.3642	0.5322	1.3965	0.5395	1.4263
0.4	0.5093	1.3462	0.5167	1.3800	0.5234	1.4113
0.6	0.4860	1.3153	0.4927	1.3519	0.4987	1.3855
0.8	0.4566	1.2704	0.4627	1.3109	0.4678	1.3479
1.0	0.4234	1.2101	0.4290	1.2559	0.4333	1.2971
1.2	0.3883	1.1333	0.3940	1.1861	0.3978	1.2326
1.4	0.3525	1.0389	0.3591	1.1011	0.3630	1.1543
1.6	0.3158	0.9254	0.3248	1.0012	0.3297	1.0629
1.8	0.2763	0.7892	0.2907	0.8871	0.2980	0.9601
2.0	0.2255	0.6044	0.2553	0.7593	0.2670	0.8482
2.2			0.2165	0.6166	0.2359	0.7306
2.4			0.1691	0.4478	0.2041	0.6115
2.6					0.1722	0.4971
2.8					0.1432	0.3982
3.0					0.1237	0.3344
π					0.1192	0.3199

Table 4 shows the values of $Nu_x \operatorname{Re}_x^{-1/2}$ and $Sh_x \operatorname{Re}_x^{-1/2}$ with various values of x and ω. It is found that opposing flow of concentration mixed convection parameter provided the separation. Further, from Table 4, the increase of ω may delayed the separation.

Figs. 2 to 9 are illustrated in order to understand the effects of parameters discussed on temperature profiles $\theta(\eta)$, velocity profiles $f'(\eta)$ and concentration profiles $\phi(\eta)$ as well as their boundary layer thicknesses at a stagnation region $(x = 0)$. From Figs.2 to 4, it was found that the increase of λ, ω and Pr reduces the thermal boundary layer thickness while the nanofluid parameter which are Le, N_b and N_t enhances the thicknesses. At the stagnation region, it is worth

mentioning that the viscous dissipation does not give any effect to the flow field as well as heat transfer characteristic.

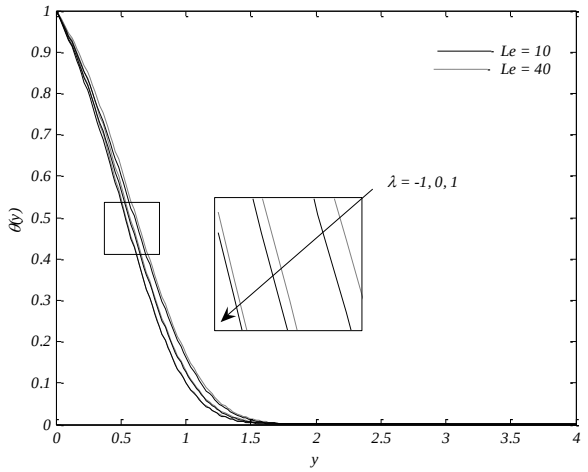

Fig. 2 Temperature profiles $\theta(y)$ against y for various values of λ and Le when $N_b = N_t = Ec = 0.1$ and $\Pr = \omega = 1$.

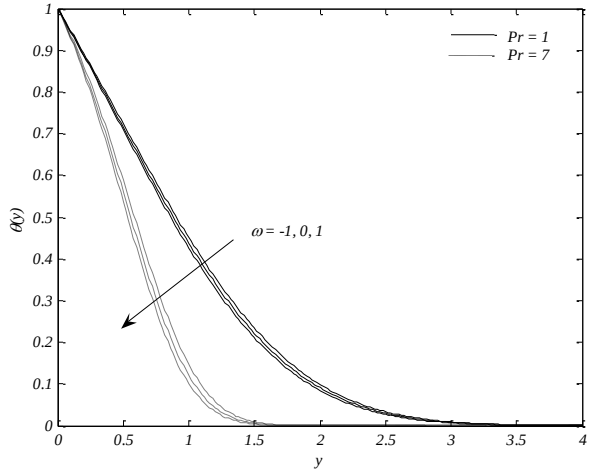

Fig. 3 Temperature profiles $\theta(y)$ against y for various values of values of Pr and ω when $\lambda = 1$, $N_b = N_t = Ec = 0.1$ and $Le = 10$.

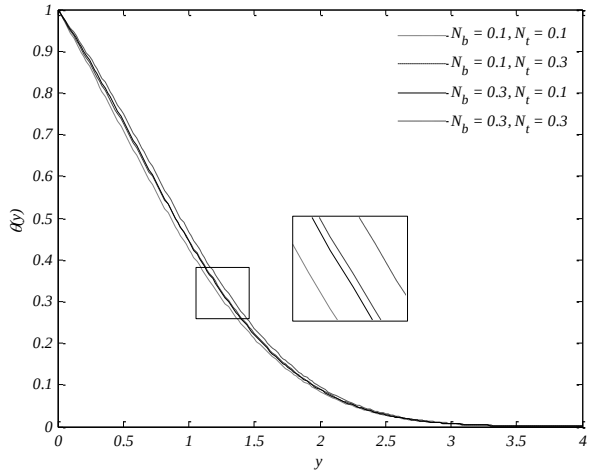

Fig. 4 Temperature profiles $\theta(y)$ against y for various values of values of N_b and N_t when $\Pr = \lambda = \omega = 1$, $Le = 10$ and $Ec = 0.1$.

Figs. 5 and 6 show the velocity profiles $f'(\eta)$ at a stagnation region $(x = 0)$ for various values of λ, Le, N_b and N_t, respectively. From Fig. 5, the increase of λ contributes to the increase of the velocity gradient which results in the increase of skin friction coefficient. Further, it is suggested that the presence of gravitational forces in the mixed convection results the increase of boundary layer thickness. It is clear from Fig. 5 that the opposing buoyancy flow $(\lambda < 0)$ contributes to the increase of boundary layer thickness. In Fig. 6, the effect of N_b and N_t is very small on velocity profiles. The increase of N_b reduced the boundary layer thickness while N_t enhanced the thicknesses.

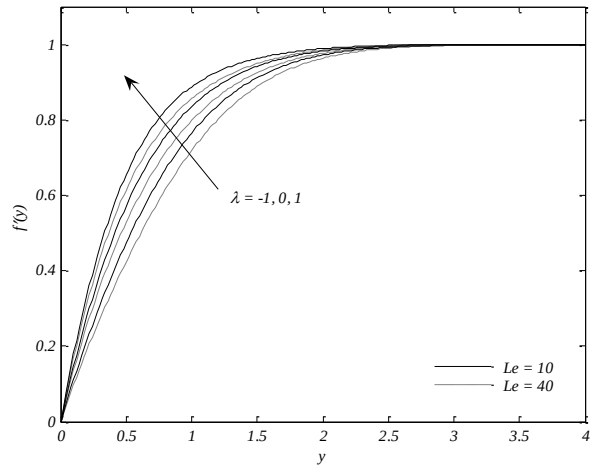

Fig. 5 Velocity profiles $f'(y)$ against y for various values of λ and Le when $N_b = N_t = Ec = 0.1$ and $\Pr = \omega = 1$.

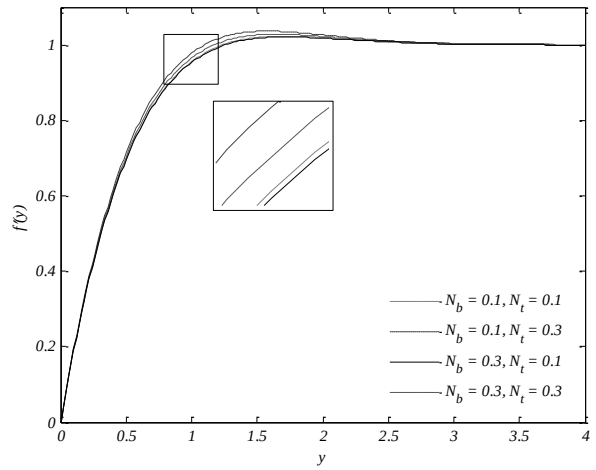

Fig. 6 Velocity profiles $f'(y)$ against y for various values of values of N_b and N_t when $\Pr = \lambda = \omega = 1$, $Le = 10$ and $Ec = 0.1$.

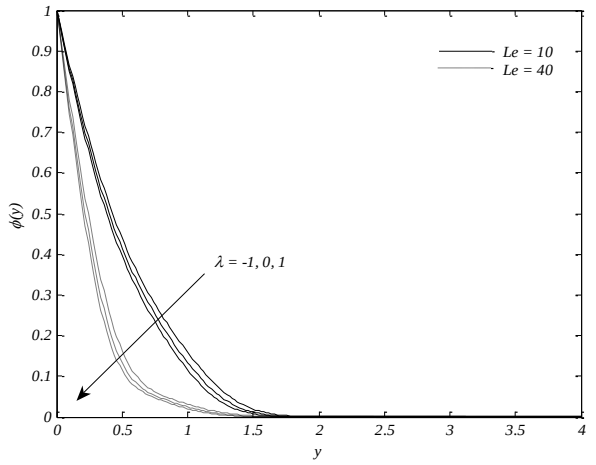

Fig. 7 Concentration profiles $\phi(y)$ against y for various values of λ and Le when $N_b = N_t = Ec = 0.1$ and $\Pr = \omega = 1$.

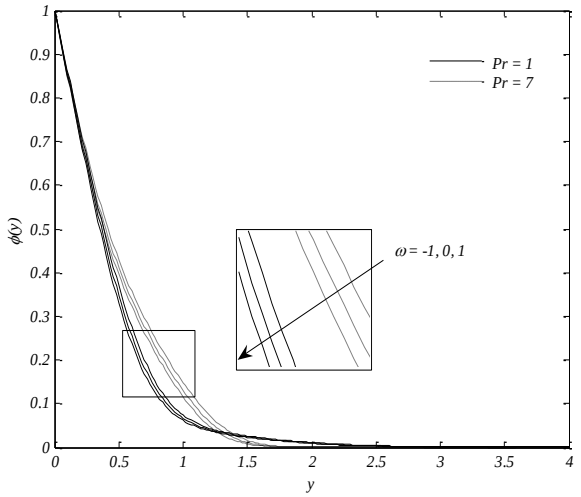

Fig. 8 Concentration profiles $\phi(y)$ against y for various values of values of Pr and ω when $\lambda = 1,\ N_b = N_t = Ec = 0.1$ and $Le = 10$.

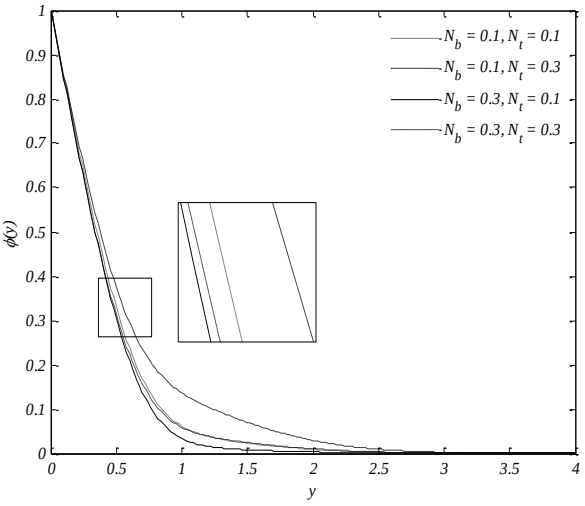

Fig. 9 Concentration profiles $\phi(y)$ against y for various values of values of N_b and N_t when $\Pr = \lambda = \omega = 1,\ Le = 10$ and $Ec = 0.1$.

The concentration profiles $\phi(\eta)$ at a stagnation region $(x = 0)$ for various values of λ, Le, $N_b, N_t, \Pr$ and ω are plotted in Figs.7 to 9, respectively. From figures, it is clearly shown that the increase of λ, Le, $N_b, \Pr$ and ω results to a decreasing of concentration. This is due to weak mass diffusivity effect compared to a thermal diffusivity in Le which lead to a reduction of volume fraction. Meanwhile, as N_t increases, the concentration increases.

Next, Figs. 10 to 13 show the variations of $Nu_x \mathrm{Re}_x^{-1/2}$ and $Sh_x \mathrm{Re}_x^{-1/2}$ for various values of N_b, N_t, Le and Ec, respectively. From Figs. 10 and 12, $Nu_x \mathrm{Re}_x^{-1/2}$ and $Sh_x \mathrm{Re}_x^{-1/2}$ decreases as the flow passes through the body of cylinder. It is seen that the increase of N_b and N_t results in a decreasing manner of $Nu_x \mathrm{Re}_x^{-1/2}$. The effects of N_b and N_t are more pronounced at the stagnation region $(x = 0)$. This is due to the no slip properties of stagnation region which allowed the maximum ability of heat and mass transfer between cylinder surface and the fluid. This property also causes zero skin friction at a stagnation region as depicted in Fig. 15. Further, the unpredictable polar of $Sh_x \mathrm{Re}_x^{-1/2}$ for various values of N_b is seen in Fig. 12. Meanwhile, as N_t increases, $Sh_x \mathrm{Re}_x^{-1/2}$ also increases.

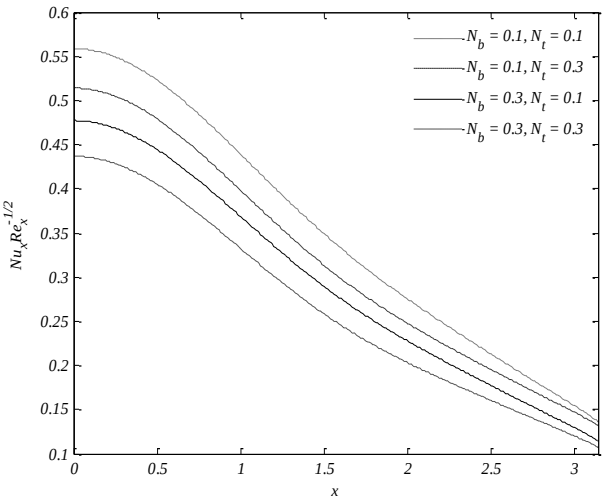

Fig. 10 Variation of $Nu_x \mathrm{Re}_x^{-1/2}$ against x for various values of N_b and N_t when $\Pr = \lambda = \omega = 1,\ Le = 10$ and $Ec = 0.1$.

In Fig. 11, it is clearly shown that at the stagnation region $(x = 0)$, $Nu_x \mathrm{Re}_x^{-1/2} = 0$ for all values of Ec. In the middle of cylinder, the effects of Ec is more pronounced. For some values of Ec ie; $Ec = -0.2$, $Nu_x \mathrm{Re}_x^{-1/2}$ increases at the middle of the cylinder before decreasing back to the end of cylinder. For $Ec \geq 0$, it is suggested that $Nu_x \mathrm{Re}_x^{-1/2}$ decreases with x along the cylinder. In summary, $Nu_x \mathrm{Re}_x^{-1/2}$ decreases as Le and Ec increases.

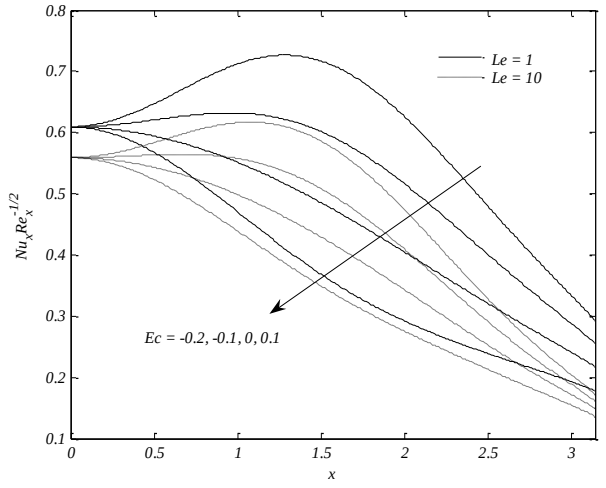

Fig. 11 Variation of $Nu_x \mathrm{Re}_x^{-1/2}$ against x for various values of Le and Ec when $\Pr = 1,\ N_b = N_t = 0.1$ and $\lambda = \omega = 1$.

Differ with Fig. 12, the increase of Le and Ec in Fig. 13 gives the increase of $Sh_x \mathrm{Re}_x^{-1/2}$. Similar trends also occur with Fig. 11, where the uniqueness of $Sh_x \mathrm{Re}_x^{-1/2}$ at a stagnation region and significance effect of Ec at the middle of the cylinder. The uniqueness $Nu_x \mathrm{Re}_x^{-1/2}$ and $Sh_x \mathrm{Re}_x^{-1/2}$ is due to the elimination of viscous dissipation effects at the stagnation region $(x = 0)$. Further, it is worth to state that the effects of Le is very large at a stagnation region where $Sh_x \mathrm{Re}_x^{-1/2}$ increases as Le increases which physically denotes enhancement of mass transfer capabilities. Lewis number Le effects is slowly decreasing as the flow passess through the cylinder.

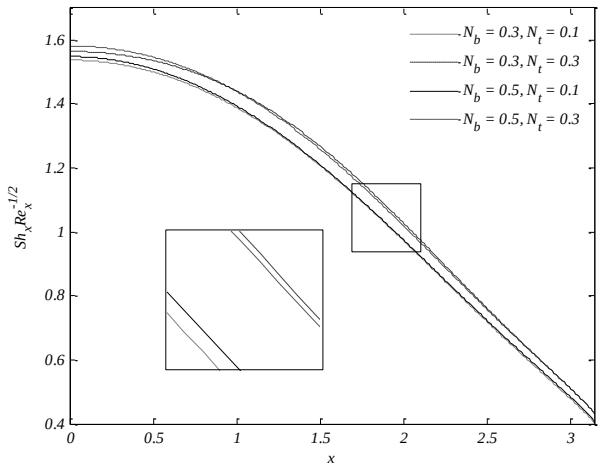

Fig. 12 Variation of $Sh_x \operatorname{Re}_x^{-1/2}$ against x for various values of N_b and N_t when $\Pr = \lambda = \omega = 1,\ Le = 10$ and $Ec = 0.1$.

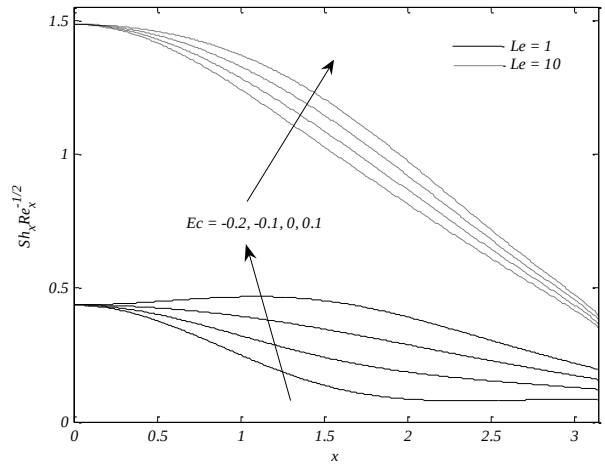

Fig. 13 Variation of $Sh_x \operatorname{Re}_x^{-1/2}$ against x for various values of Le and Ec when $\Pr = 1,\ N_b = N_t = 0.1$ and $\lambda = \omega = 1$.

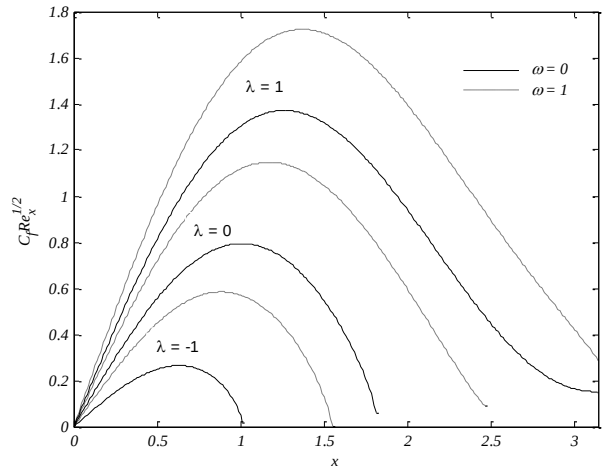

Fig. 14 Variation of $C_f \operatorname{Re}_x^{1/2}$ against x for various values of λ and ω when $\Pr = 1,\ N_b = N_t = Ec = 0.1$ and $Le = 10$.

Lastly, Figs. 14 to 16 displayed the variation of $C_f \operatorname{Re}_x^{1/2}$ against x for various values of parameters. From Fig. 14, for all λ, it is found that $C_f \operatorname{Re}_x^{1/2}$ is unique $\left(C_f \operatorname{Re}_x^{1/2} = 0\right)$ at a stagnation region before increasing dramatically as x increases. For λ which has a separation point, $C_f \operatorname{Re}_x^{1/2}$ is then decreased back to approach 0 just before it reaches the separation value. Note that, the increase of λ results in the increase of $C_f \operatorname{Re}_x^{1/2}$ at any point of x. Next, it is noticed that the presence of assisting buoyant for concentration $(\omega > 0)$ has delayed the separation to occured. From numerical analysis, for $\lambda = -1$, in the absence of ω, the separation occur as early at $x = 1.01$. The presence of ω $(\omega = 1)$ has delayed the separation to $x = 1.55$.

In Figs. 15 and 16, it was found that at the early stage of the cylinder, $C_f \operatorname{Re}_x^{1/2}$ is unique for all parameter N_b, N_t, Le and Ec. The effects of N_b, N_t, Le and Ec are more pronounced as x increases to the middle until to the end of cylinder body. Further, it is clearly shown that the increase of N_t and Ec results in the increase of $C_f \operatorname{Re}_x^{1/2}$ while N_b and Le does contrary. It is suggested that in convective boundary layer flow on horizontal circular cylinder, these no skin friction $\left(C_f \operatorname{Re}_x^{1/2} = 0\right)$ that occurs at a stagnation region due to the no slip effect and $C_f \operatorname{Re}_x^{1/2}$ tends to be maximum at the middle of the cylinder due to the slip effect properties before decreasing back as fluid flow through the end of cylinder body.

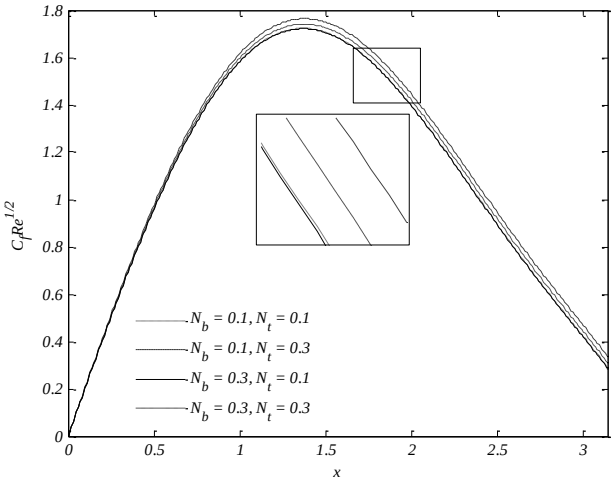

Fig. 15 Variation of $C_f \operatorname{Re}_x^{1/2}$ against x for various values of N_b and N_t when $\Pr = \lambda = \omega = 1,\ Le = 10$ and $Ec = 0.1$.

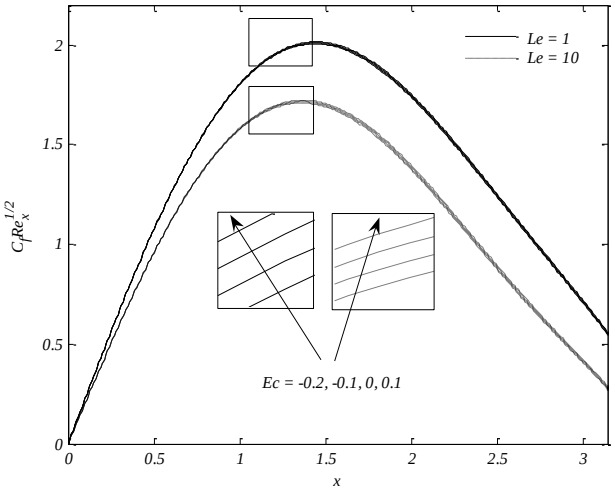

Fig. 16 Variation of $C_f \operatorname{Re}_x^{1/2}$ against x for various values of Le and Ec when $\Pr = 1,\ N_b = N_t = 0.1$ and $\lambda = \omega = 1$.

CONCLUSION

In this paper, the problem of mixed convection boundary layer flow on a horizontal circular cylinder in a nanofluid with viscous dissipation effects and constant wall temperature is numerically studied. It was found that the present of gravitational forces in mixed convection parameter λ and ω results in the increase of the velocity gradient at the surface, and thus increase the skin friction coefficient beside delayed the flow separation. As the flow passes through the cylinder, the skin friction coefficient increased from origin to the middle of the cylinder before decreasing back to the end of cylinder. Finally, the presence of gravitational forces has also increased the velocity boundary layer thickness in opposing flow.

Furthermore, the increase in the thermophoresis parameter N_t, Lewis number Le and Eckert number Ec results in the increase of Sherwood number while Nusselt number decreased which physically denoted as the enhancement in mass transfer capabilities while reduced the convective heat transfer capabilities.

At the stagnation region, the value of skin friction coefficient is unique for all parameters N_b, N_t, Le and Ec. The effects of N_b, N_t, Le and Ec are more pronounced as x increases to the middle until to the end of the cylinder body.

ACKNOWLEDGEMENT

The authors would like to thank the DRB-HICOM University of Automotive Malaysia and Universiti Malaysia Pahang for the financial, facilities and moral support.

REFERENCES

Ahmad, S., Arifin, N. M., Nazar, R. & Pop, I. (2009). Mixed convection boundary layer flow past an isothermal horizontal circular cylinder with temperature-dependent viscosity. *International Journal of Thermal Sciences*, 48(10), 1943-1948.

Aldoss, T. K., Ali, Y. D. & Al-Nimr, M. A. (1996). MHD mixed convection from a horizontal circular cylinder. *Numerical Heat Transfer, Part A: Applications*, 30(4), 379-396.

Anwar, I., Amin, N. & Pop, I. (2008). Mixed convection boundary layer flow of a viscoelastic fluid over a horizontal circular cylinder. *International Journal of Non-Linear Mechanics*, 43(9), 814-821.

Anwar, I., Qasim, A. R., Ismail, Z., Salleh, M. Z. & Shafie, S. (2013). Chemical reaction and uniform heat generation/absorption effects on MHD stagnation-point flow of a nanofluid over a porous sheet. *World Applied Sciences Journal*, 24(10), 1390-1398.

Gebhart, B. (1962). Effects of viscous dissipation in natural convection. *Journal of Fluid Mechanics*, 14(02), 225-232.

Hussanan, A., Khan, I., Hashim, H., Mohamed, M. K. A., Ishak, N., Sarif, N. M. & Salleh, M. Z. (2016). Unsteady MHD flow of some nanofluids past an accelerated vertical plate embedded in a porous medium. *Jurnal Teknologi*, 78(2), 121-126.

Jain, P. & Lohar, B. (1979). Unsteady mixed convection heat transfer from a horizontal circular cylinder. *Journal Heat Transfer*, 101(1), 126-131.

Jan, S. A. A., Ali, F., Sheikh, N. A., Khan, I., Saqib, M. & Gohar, M. (2017). Engine oil based generalized brinkman-type nano-liquid with molybdenum disulphide nanoparticles of spherical shape: Atangana-Baleanu fractional model. *Numerical Methods for Partial Differential Equations*, 00, 1-17.

Khan, I. (2017). Shape effects of MoS_2 nanoparticles on MHD slip flow of molybdenum disulphide nanofluid in a porous medium. *Journal of Molecular Liquids*, 233, 442-451.

Kho, Y. B., Hussanan, A., Mohamed, M. K. A., Sarif, N. M., Ismail, Z. & Salleh, M. Z. (2017). Thermal radiation effect on MHD Flow and heat transfer analysis of Williamson nanofluid past over a stretching sheet with constant wall temperature. *Journal of Physics: Conference Series*, 890(1), 1-6.

Kumari, M. & Nath, G. (1989). Unsteady mixed convection with double diffusion over a horizontal cylinder and a sphere within a porous medium. *Wärme−und Stoffübertragung*, 24, 103-109.

Merkin, J. H. (1977). Mixed convection from a horizontal circular cylinder. *International Journal of Heat and Mass Transfer*, 20(1), 73-77.

Mohamed, M. K. A., Noar, N. A. Z., Salleh, M. Z. & Ishak, A. 2015. Stagnation point flow past a stretching sheet in a nanofluid with slip condition. *AIP Proceedings of International Statistical Conference (ISM-II)*, 1643, 635-641.

Mohamed, M. K. A., Noar, N. A. Z., Salleh, M. Z. & Ishak, A. (2016). Free convection boundary layer flow on a horizontal circular cylinder in a nanofluid with viscous dissipation. *Sains Malaysiana*, 45(2), 289-296.

Nazar, R. 2003. Mathematical model for free and mixed convection boundary layer flows of micropolar fluids. Ph.D. Thesis, Universiti Teknologi Malaysia.

Nazar, R., Amin, N. & Pop, I. (2003). Mixed convection boundary-layer flow from a horizontal circular cylinder in micropolar fluids: case of constant wall temperature. *International Journal of Numerical Methods for Heat & Fluid Flow*, 13(1), 86-109.

Nazar, R., Tham, L., Pop, I. & Ingham, D. (2011). Mixed convection boundary layer flow from a horizontal circular cylinder embedded in a porous medium filled with a nanofluid. *Transport in Porous Media*, 86(2), 517-536.

Rashad, A. M., Chamkha, A. J. & Modather, M. (2013). Mixed convection boundary-layer flow past a horizontal circular cylinder embedded in a porous medium filled with a nanofluid under convective boundary condition. *Computers & Fluids*, 86, 380-388.

Roşca, A. V., Roşca, N. C. & Pop, I. (2014). Note on dual solutions for the mixed convection boundary layer flow close to the lower stagnation point of a horizontal circular cylinder: Case of constant surface heat flux. *Sains Malaysiana*, 43(8), 1239-1247.

Roşca, N. C. & Pop, I. (2014). Unsteady boundary layer flow of a nanofluid past a moving surface in an external uniform free stream using Buongiorno's model. *Computers & Fluids*, 95, 49-55.

Salleh, M. Z., Nazar, R. & Pop, I. (2010). Mixed convection boundary layer flow over a horizontal circular cylinder with Newtonian heating. *Heat and Mass Transfer*, 46(11-12), 1411-1418.

Tham, L. & Nazar, R. (2012). Mixed convection flow about a solid sphere embedded in a porous medium filled with a nanofluid. *Sains Malaysiana*, 41(12), 1643-1649.

Udhayakumar, S., Abin Rejeesh, A. D., Sekhar, T. V. S. & Sivakumar, R. (2016). Numerical investigation of magnetohydrodynamic mixed convection over an isothermal circular cylinder in presence of an aligned magnetic field. *International Journal of Heat and Mass Transfer*, 95, 379-392.

Wong, K. V. & De Leon, O. (2010). Applications of Nanofluids: Current and Future. *Advances in Mechanical Engineering*, 2010, 1-11.